Journal of Virology®

VIRUS-CELL INTERACTIONS

Exploitation of a Bacterium-Encoded Lytic Transglycosylase by a Human Oral Lytic Phage To Facilitate Infection

Lujia Cen,[a] Yunjie Chang,[b] Joseph K. Bedree,[a] Yansong Ma,[c] Qiu Zhong,[d] Daniel R. Utter,[e] Pu-Ting Dong,[a] Renate Lux,[f] Batbileg Bor,[a,g] Jun Liu,[b] Jeffrey S. McLean,[h] Shuai Le,[d] Xuesong He[a,g]

[a]Department of Microbiology, The Forsyth Institute, Cambridge, Massachusetts, USA
[b]Microbial Sciences Institute, Yale University, New Haven, Connecticut, USA
[c]Capital University of Medicine, Beijing, China
[d]Department of Microbiology, Army Medical University, Chongqing, China
[e]Division of Geological and Planetary Sciences, California Institute of Technology, Pasadena, California, USA
[f]Section of Biosystems and Function, UCLA School of Dentistry, Los Angeles, California, USA
[g]Department of Oral Medicine, Infection and Immunity, Harvard School of Dental Medicine, Boston, Massachusetts, USA
[h]Department of Periodontics, University of Washington, Seattle, Washington, USA

ABSTRACT Bacteriophages (phages) are an integral part of the human oral microbiome. Their roles in modulating bacterial physiology and shaping microbial communities have been discussed but remain understudied due to limited isolation and characterization of oral phage. Here, we report the isolation of LC001, a lytic phage targeting human oral *Schaalia odontolytica* (formerly known as *Actinomyces odontolyticus*) strain XH001. We showed that LC001 attached to and infected surface-grown, but not planktonic, XH001 cells, and it displayed remarkable host specificity at the strain level. Whole-genome sequencing of spontaneous LC001-resistant, surface-grown XH001 mutants revealed that the majority of the mutants carry nonsense or frameshift mutations in XH001 gene *APY09_05145* (renamed *ltg-1*), which encodes a putative lytic transglycosylase (LT). The mutants are defective in LC001 binding, as revealed by direct visualization of the significantly reduced attachment of phage particles to the XH001 spontaneous mutants compared that to the wild type. Meanwhile, targeted deletion of *ltg-1* produced a mutant that is defective in LC001 binding and resistant to LC001 infection even as surface-grown cells, while complementation of *ltg-1* in the mutant background restored the LC001-sensitive phenotype. Intriguingly, similar expression levels of *ltg-1* were observed in surface-grown and planktonic XH001, which displayed LC001-binding and nonbinding phenotypes, respectively. Furthermore, the overexpression of *ltg-1* failed to confer an LC001-binding and -sensitive phenotype to planktonic XH001. Thus, our data suggested that rather than directly serving as a phage receptor, *ltg-1*-encoded LT may increase the accessibility of phage receptor, possibly via its enzymatic activity, by cleaving the peptidoglycan structure for better receptor exposure during peptidoglycan remodeling, a function that can be exploited by LC001 to facilitate infection.

IMPORTANCE The evidence for the presence of a diverse and abundant phage population in the host-associated oral microbiome came largely from metagenomic analysis or the observation of virus-like particles within saliva/plaque samples, while the isolation of oral phage and investigation of their interaction with bacterial hosts are limited. Here, we report the isolation of LC001, the first lytic phage targeting oral *Schaalia odontolytica*. Our study suggested that LC001 may exploit the host bacterium-encoded lytic transglycosylase function to gain access to the receptor, thus facilitating its infection.

KEYWORDS oral lytic phage, lytic transglycosylase, oral microbiome, bacterial phage interaction

Editor Anice C. Lowen, Emory University School of Medicine

Address correspondence to Xuesong He, xhe@forsyth.org.

The authors declare no conflict of interest.

Received 8 July 2022
Accepted 5 August 2022

Bacteriophages (phages) are an integral component of most, if not all, microbial communities (1). They are viruses that attack bacteria and can alter competition among bacterial strains. Environmental microbial community-based studies strongly indicate that the bacterium-phage interaction is an important driver of ecological and evolutionary processes which helps maintain phenotypic and genetic diversity within microbial communities by shaping microbial structure and ecology (2, 3). Most of the studies on host microbiome-associated phages have been done with the gut microbial community. While diverse phage elements have been identified within the gut microbial community (4–6), a detailed understanding of the dynamics of phage populations, their interaction with the human microbiome, and ultimately their impact on human health still remain largely elusive.

In the oral microbiome, bacteria have been an intensive research focus since the birth of microbiology (7), with over 70% of the bacteria (close to 800 species) now successfully isolated and characterized (8). In contrast, phages remain one of the poorly understood elements due to the challenges in their identification, isolation, and characterization (9). Since the isolation of the first *Lactobacillus casei* phage from the oral cavity in 1958 (10), only a limited number of phages targeting *Actinobacillus actinomycetemcomitans* (11), *Enterococcus faecalis* (12), *Veillonella* spp. (13), *Streptococcus* spp. (14), *Fusobacterium* spp. (15), *Treponema* spp. (16), and *Actinomyces* spp. (17) have been characterized. Their potential application in targeting oral pathogens and achieving biocontrol of oral biofilm has been discussed and explored (18). Recent culture-independent, sequencing-based analyses have uncovered a vast diversity of phages and greatly expanded the landscape of phage components within the oral microbiome (19–22). Similar to bacteria, the oral phage communities present in different individuals are personal and resilient (19) and show strong biogeography within the oral microbiome (23). Meanwhile, the composition of these oral phage communities shifts during disease along with the oral microbiome composition, and this phage dysbiosis may potentially promote oral diseases (19). However, the ecological and physiological role of phages in the oral microbiome and their impact on host-microbe interactions remain obscure due to the limited number of phages that have been experimentally characterized, as well as a lack of available model systems (23).

Schaalia odontolytica, formerly known as *Actinomyces odontolyticus*, is a major commensal bacterial species residing in the human oral cavity. *Schaalia odontolytica* subsp. *actinosynbacter* strain XH001 (herein referred to as XH001) was isolated from a human saliva sample (24) and can serve as a host for the nanosized obligate bacterial epibiont "*Candidatus* Nanosynbacter lyticus" strain TM7x (24–26), an oral saccharibacterial strain that belongs to a recently described bacterial superphylum, Candidate Phyla Radiation (27). In this study, we report the isolation and characterization of a lytic phage (named LC001) that targets XH001. Our data suggest that phage LC001 may exploit an XH001-encoded lytic transglycosylase function to get access to the receptor, thus facilitating its binding and infection.

RESULTS

Isolation and characterization of LC001, an oral lytic phage of *Schaalia odontolytica* subsp. *actinosynbacter* strain XH001. LC001 induced a lysis zone on a lawn of XH001 cells in the plaque assay (Fig. 1A). Interestingly, during the phage adsorption assay, while LC001 effectively bound to surface-grown (on agar surface) XH001 cells, it failed to adsorb to planktonic cells (see Fig. S1 in the supplemental material). Thus, unless specified, surface-grown XH001 and its derivatives were used when investigating phage adsorption-related phenotypes. Cryo-electron tomography (cryo-ET) combined with cryo-focused ion beam (cryo-FIB) milling showed that LC001 attaches to the cell wall of surface-grown XH001 (Fig. 1B). To obtain structural details of LC001, we froze pure LC001 phage particles, collected tomograms, and carried out subtomogram averaging. The result showed that LC001 has an icosahedral capsid with a long tail, suggesting that it belongs to the *Siphoviridae* family. The sizes for the capsid and the tail were estimated to be 67 nm in diameter and 140 nm in length, respectively (Fig. 1C to E).

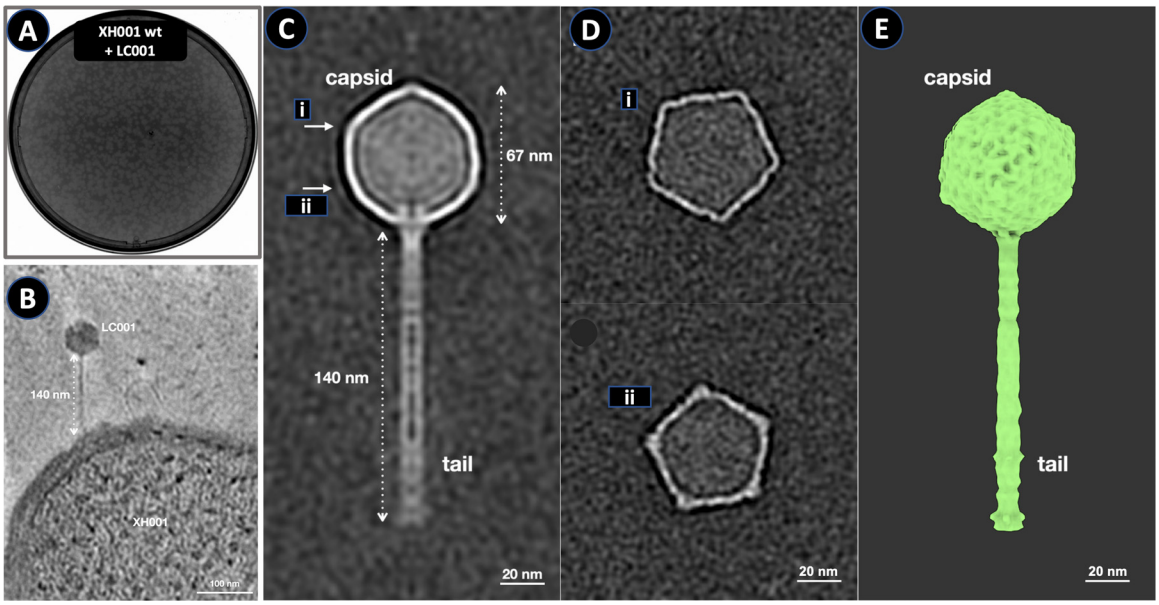

FIG 1 Lytic phage LC001. (A) Plaque assay of LC001 infecting *Schaalia odontolytica* strain XH00. (B) Cryo-EM image of LC001 attached to XH001. A section of the tomogram was recorded from the lamella of LC001-infected XH001. (C) Central slice of the subtomogram average of LC001. (D) Cross-sections (at positions i and ii labeled in panel C) showing the top views of the LC001 capsid. (E) 3D surface view of the subtomogram average of LC001.

A panel of two additional *Schaalia odontolytica* strains, F0309 and ATCC 17982, and five *Actinomyces* spp. that are phylogenetically closely related to XH001 (27) were tested against LC001 to investigate its host range. Interestingly, LC001 induces lysis only in XH001, not in any of the other tested strains, suggesting a remarkable host specificity at the strain level (Fig. S2).

Genomic analysis of LC001. The LC001 genome is comprised of 26,219 bp, with a GC content of 65.76%, similar to its host, XH001, which has an overall G+C content of 65.9%. It has a total of 43 putative open reading frames (ORFs), 25 of which were functionally annotated by protein BLAST (Fig. 2) (Table S3). The remaining 18 ORFs share little similarity to sequences available in databases at either the nucleotide or amino acid level. The annotated proteins can be classified into the following groups: structural proteins (capsid and tail proteins), packaging proteins (large terminase and a phage portal protein), DNA replication and modification proteins (replication protein O and a single-stranded DNA binding protein), and host cell lysis proteins (CHAP domain-containing protein) (Table S3).

Spontaneous LC001-resistant mutants carry a nonsense or frameshift mutation in the XH001 *APY09_05145* gene. Spontaneous LC001-resistant mutants of XH001 were selected by plating the XH001 wild type (WT) and LC001 mixture on agar medium and screening for viable colonies as described in Materials and Methods. A total of 20 colonies were picked. Eighteen of them showed normal growth, while the other two displayed growth defects. Ten mutants with normal growth were then chosen for further analysis.

Comparative genomic analysis revealed that all 10 LC001-resistant mutants with normal growth were mutated in one specific XH001 gene, *APY09_05145*. Among these mutants, eight carried nonsense mutations at various locations within the gene that would result in a truncated protein due to the introduced stop codon, while two mutants displayed a 1-bp deletion at nucleotide (nt) positions 289 and 435 within the *APY09_05145* gene, respectively, leading to a frameshift mutation (Table S4).

XH001 *APY09_05145* encodes a putative lytic transglycosylase. A BLAST search suggested that *APY09_05145* encodes a putative lytic transglycosylase (LT). The LTs are bacterial enzymes that catalyze the nonhydrolytic cleavage of the peptidoglycan (PG) structure of the bacterial cell wall (28). Thus, *APY09_05145* was renamed *ltg-1*, and its encoded protein was renamed Ltg-1. Figure 3A depicts the domain organization of

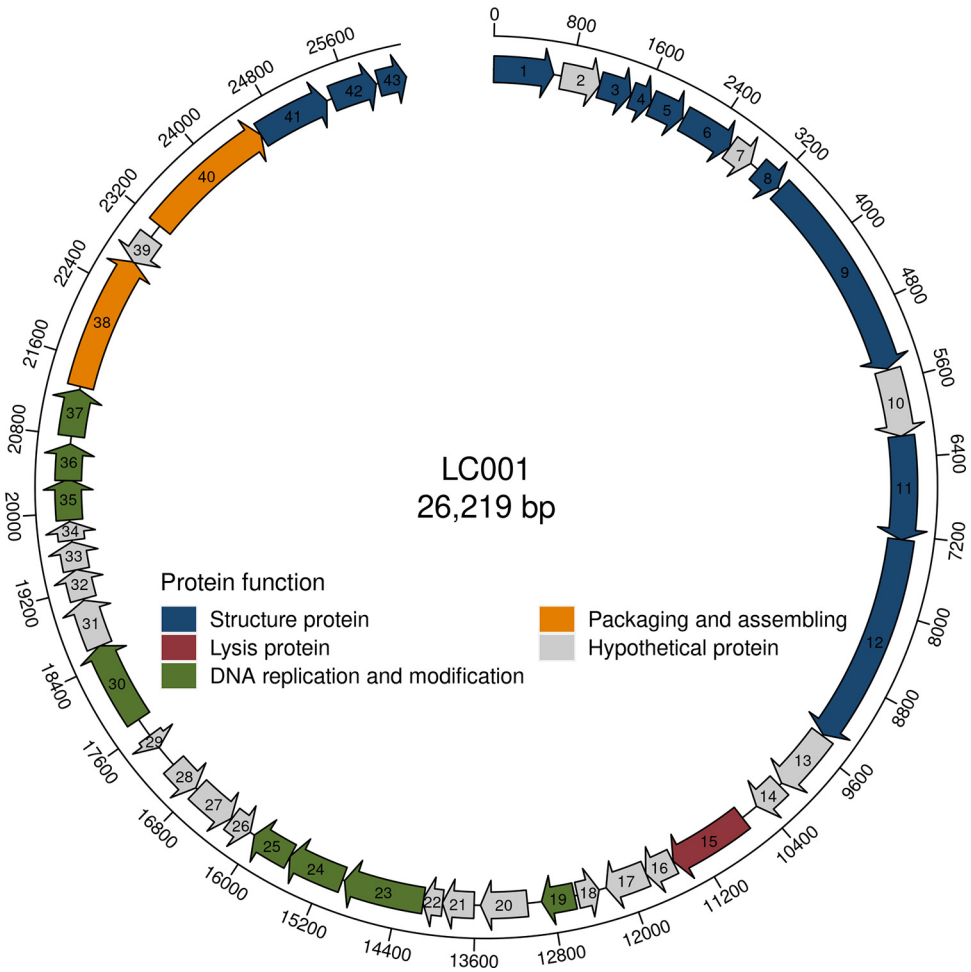

FIG 2 Schematic representation of the organization of LC001. ORFs that are classified in the same functional categories are shown in the same color. ORFs in gray encode hypothetical proteins.

Ltg-1 predicted using InterProScan (29). Ltg-1 exhibits high structural complexity, as it contains 7 predicted domains: one cytoplasmic domain at the N terminus, a helix transmembrane (TM) domain, followed by three DUF348 domains (domains of unknown function), one G5 domain, and the transglycosylase catalytic domain at the C terminus (Fig. 3A). The arrangement of the predicted domains of Ltg-1 is highly similar to that of RpfB (30), a mycobacterium-encoded lytic transglycosylase, also referred to as resuscitation-promoting factor (Fig. S3) (31). Based on the presence of a predicted helix TM domain, Ltg-1 is likely a member of the membrane-bound family 3 of LTs (32).

We then focused on the predicted catalytic function of Ltg-1 and aligned the predicted transglycosylase domain with the one present in *Escherichia coli* SltY. SltY is a family 3 type LT, and its crystal structure has been determined (33–36). The active-site amino acid is glutamate at position 478; changing this residue to glutamine abolishes enzyme activity. The alignment showed that while the overall sequence similarity between SltY and XH001 LT is relatively low, the catalytic glutamate and the amino acids important in forming the active site are well conserved (Fig. 3B). Genome-wide searches of XH001 revealed the presence of at least two additional genes encoding putative LT. One is *APY09_05140*, which encodes a protein that also shares domain-level similarity to *Mycobacterium tuberculosis* RpfB and is predicted to be a member of family 1 type LTs, and the other is *APY09_08845* (Fig. S3).

Spontaneous LC001-resistant mutants are defective in phage binding. To investigate whether the LC001-resistant phenotype is due to an impairment of the mutant's

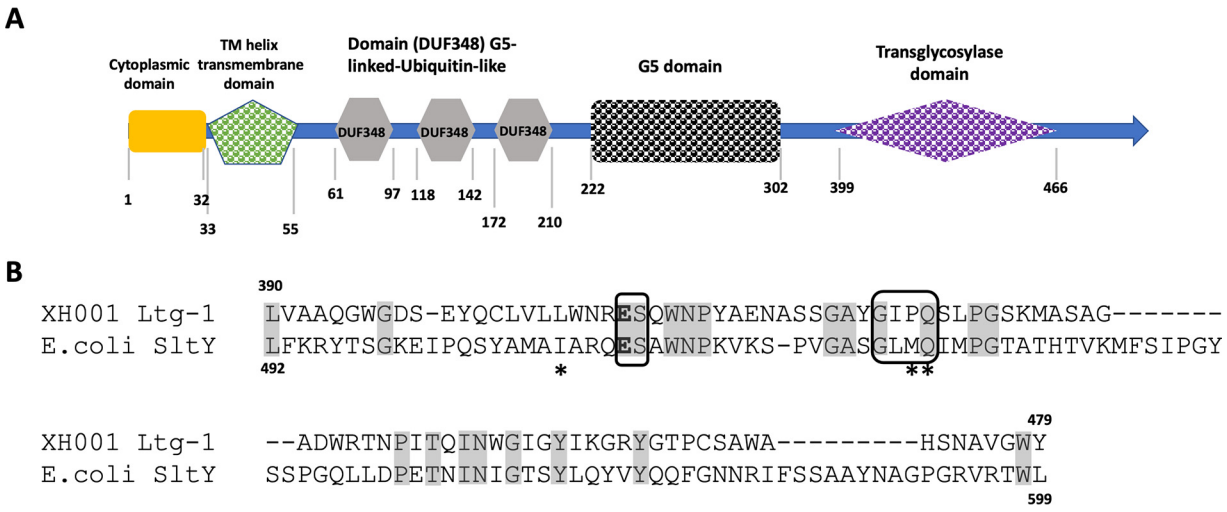

FIG 3 Analysis of *ltg-1*-encoded protein. (A) Predicted domain organization of Ltg-1 using InterProScan. (B) Alignment of residues 390 to 479 of XH001 Ltg-1 with residues 492 to 599 of *E. coli* lytic transglycosylase SltY. Identical residues are shaded, conserved motifs important for the architecture of the active site are boxed, and the catalytic glutamate of SltY and its counterpart in Ltg-1 are in bold. Asterisks indicate hydrophobic residues of SltY that surround the catalytic glutamate.

ability in phage binding, one of the spontaneous mutants, named XH001 LR-01, which has a nonsense mutation in *APY09_05145*, was chosen for further analysis. XH001 LR-01 carries a C-to-A transversion mutation at nucleotide position 125/1440 in the *APY09_05145* gene, which caused a nonsense mutation by introducing a stop codon (TAG) to replace a serine-encoding TCG, and the mutant displayed growth dynamics and cell morphology similar to that of the wild type (Fig. S4).

SYBR green-tagged LC001 was mixed with Laurdan-labeled XH001 LR-01, and the binding between phage and bacteria was directly visualized microscopically. The data showed significant colocalization of SYBR green and Laurdan signal when phage particles were mixed with XH001 wild type, indicative of direct physical binding between phage and bacteria. In contrast, there was a significant decrease in the colocalization of the two signals when SYBR green-tagged LC001 was mixed with Laurdan-labeled XH001 LR-01, suggesting reduced binding between LC001 and XH001 LR-01 (Fig. 4A and B). This is consistent with the plaque assay data showing that LC001 failed to induce cell lysis in XH001 LR-01, as reflected by the absence of plaque formation on the agar plates (Fig. 4C).

Targeted *ltg-1* deletion in XH001 leads to a defect in phage binding and an LC001-resistant phenotype. To confirm that the *ltg-1*-encoded function is required for successful LC001 adsorption and infection, we generated an *ltg-1* deletion mutation in the XH001 wild-type background (named XH001 Δ*ltg-1*) via targeted allelic replacement as described in Materials and Methods and depicted in Fig. S5. As expected, surface-grown XH001 Δ*ltg-1* displayed significantly reduced phage binding and is resistant to LC001 infection, phenotypes similar to the ones observed for the spontaneously LC001-resistant mutant XH001 LR-01 (Fig. 4A to C).

Complementation of XH001 LR-01 with an *ltg-1*-expressing plasmid restores an LC001-sensitive phenotype. To further confirm that the *ltg-1*-encoded function is indeed critical for LC001 infection, we performed a complementation experiment by introducing pCLJ100 (Fig. 5A), a pJRD215 derivative expressing XH001 *ltg-1*, into the LC001-sensitive mutant XH001 LR-01. The successful transformation was confirmed by diagnostic PCR (Fig. 5B). A phage sensitivity assay clearly showed that XH001 LR-01 reverted to the LC001-sensitive phenotype when carrying the *ltg-1*-expressing plasmid pCLJ100 (Fig. 5C).

***ltg-1* expression levels are similar in surface- and planktonically grown XH001 cells.** Ltg-1 is predicted to be a membrane-bound family 3 LT, and data so far seemingly suggest that it could serve as a receptor for direct LC001 binding. However,

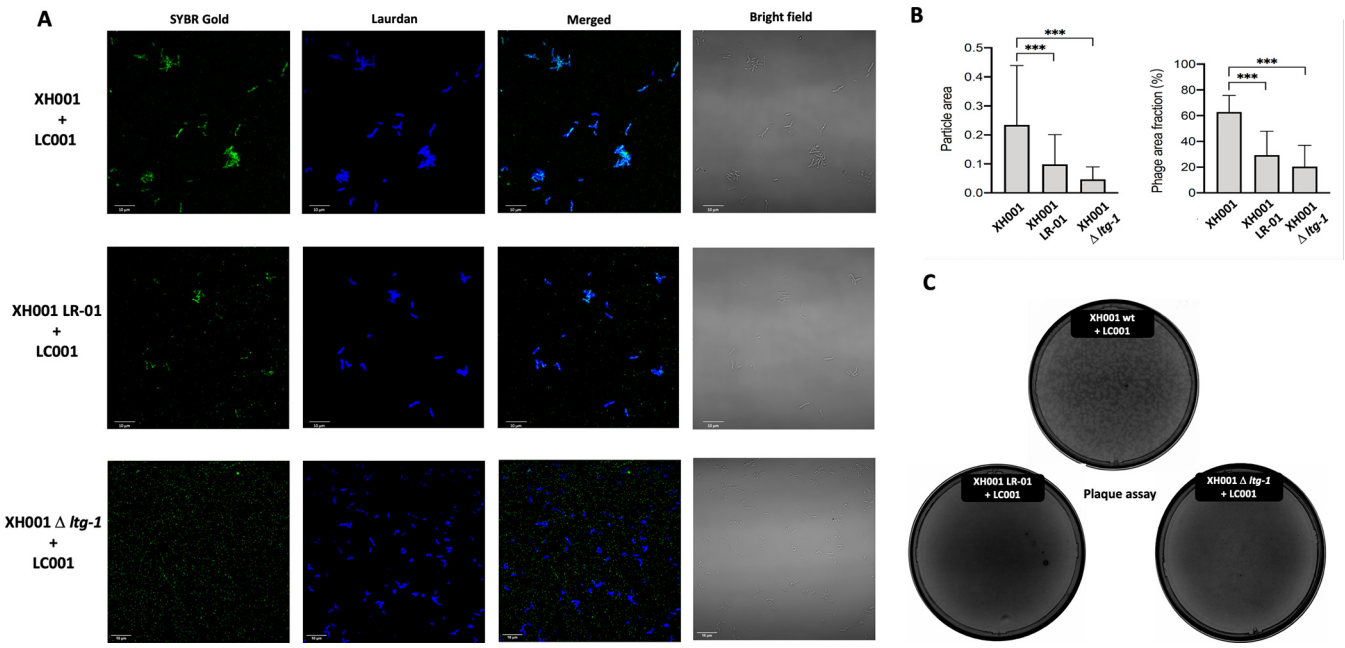

FIG 4 Visualization of attachment of SYBR green-labeled phage to XH001 WT and different mutants. (A) Microscopic observation of binding between SYBR green-tagged LC001 and Laurdan-labeled XH001. (B) Quantification of LC001 binding to XH001 WT and mutants by Fiji particle analysis. (C) Plaque assay of LC001 infecting *Schaalia odontolytica* strain XH001 WT and different mutants.

among the limited number of identified receptors for Gram-positive bacterium-targeting phages, the majority are associated with either PG or teichoic acid structure but are not proteinaceous in nature (37). Furthermore, it has been reported that an *Escherichia coli*-encoded LT is required for effective phage infection during its stationary-phase growth, likely through its enzymatic function that helps phage to overcome a thickened PG barrier during stationary phase and facilitate infection (38). Since XH001 cells displayed a drastic difference in phage binding when they were grown planktonically and when they were surface grown (Fig. S1), we reasoned that if Ltg-1 indeed serves as a receptor for LC001 binding, a differential expression in *ltg-1* might be observed under these two conditions. However, the quantitative real-time reverse transcription PCR (qRT-PCR) data revealed similar *ltg-1* gene expression levels when cells were in two different growth modes (Fig. 6A). Furthermore, we showed that the introduction of pCLJ100, an *ltg-1*-expressing plasmid that can restore the phage-binding and LC001-sensitive phenotype in XH001 LR-01 (Fig. 4A and B), did not enhance planktonic XH001 cells' LC001 adsorption (Fig. 6B). These data argue against the possibility that Ltg-1 directly serves as a receptor for LC001.

DISCUSSION

In this study, we report the isolation and characterization of an oral lytic phage, LC001, targeting the commensal bacterial isolate *S. odontolytica* strain XH001 (Fig. 1). The genetic and phenotypic analyses demonstrated that the XH001-encoded lytic transglycosylase (LT) function is likely to be exploited by LC001 to facilitate its binding and infection (38).

Genomic sequencing identified the XH001 gene encoding lytic transglycosylase, named *ltg-1*, as critical for LC001 binding and the LC001-sensitive phenotype when cells were growing on the agar surface. Mutation in *ltg-1* led to defects in phage binding and the LC001-resistant phenotype (Fig. 4), while complementation of *ltg-1* restored the mutant's sensitivity to phage (Fig. 5). While these data seem to suggest that Ltg-1 could potentially serve as an LC001 receptor, a few lines of evidence argue against it. First, few phage receptors have been identified and characterized thus far for Gram-positive bacteria due to the complexity of cell walls containing different moieties that can contribute to phage

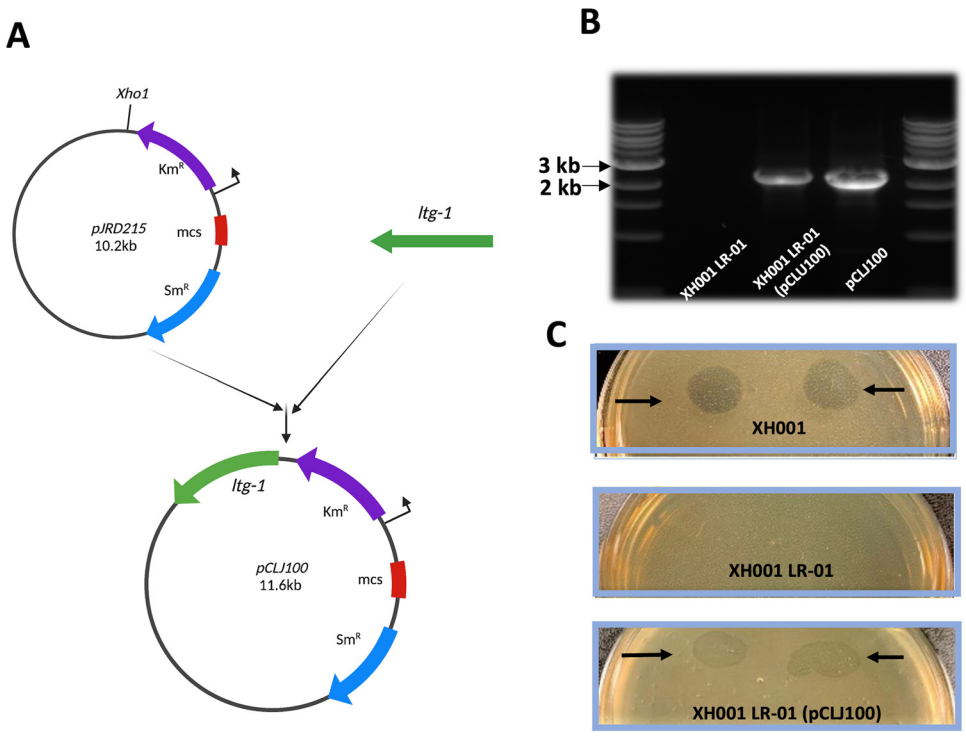

FIG 5 *ltg-1* gene complementation. (A) Schematic map showing generation of *ltg-1*-expressing pCLJ100. (B) Conformation of the XH001 LR-01 transformant carrying pCLJ100 plasmid. (C) Spot-test lysis assay. Arrow indicates the lysis zone. mcs, multiple-cloning sites.

adsorption. Among the limited number of identified receptors for Gram-positive bacteria, the majority are associated with either PG or teichoic acid structure but are not proteinaceous in nature (37). Second, XH001 cells grown planktonically and those grown on the agar surface showed a drastic difference in phage binding. Dissimilar binding of phage onto bacterial surfaces often results from differential expression of bacterially encoded phage receptors (39). Our RT-qPCR data, however, did not reveal any significant change in *ltg-1* expression between planktonically and surface-grown XH001 cells (Fig. 6A). Lastly, overexpression of the *ltg-1* gene did not enhance LC001 binding to planktonic XH001 cells (Fig. 6B). Thus, while a definitive conclusion may not be drawn, our findings argue against Ltg-1 serving directly as a receptor for LC001.

During phage infection, the irreversible binding and ejection of phage genetic ma-

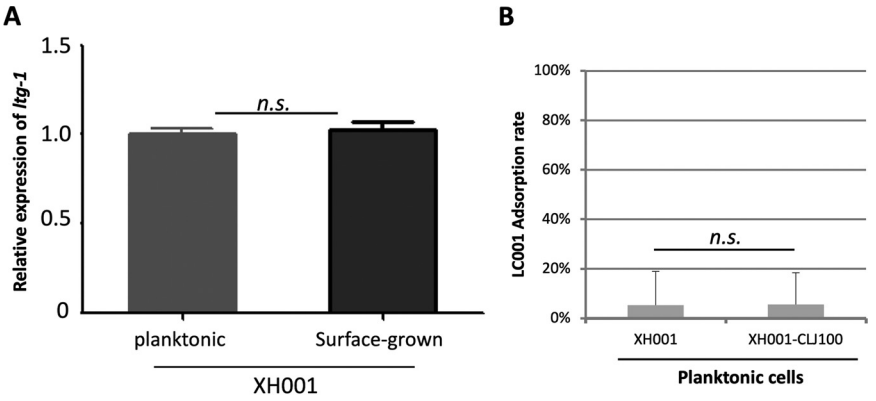

FIG 6 *ltg-1* expression and phage adsorption. (A) RT-qPCR analysis determining the relative expression level of *ltg-1* in planktonic versus surface-grown (on agar surface) XH001 WT. (B) LC001 adsorption assay comparing the phage adsorption rates between planktonically grown cells of XH001 WT and XH001-CLJ100 that overexpresses the *lgt-1* gene. n.s., not statistically significant.

terial must be preceded by the successful passage of diverse carbohydrate barriers of the host, including the thick PG layers in Gram-positive bacteria, such as *S. odontolytica*. Many phages targeting Gram-positive bacteria encode virion-associated lysins (VALs), including glycosidases (such as lysozyme and lytic transglycosylase), amidase, and/or endopeptidase (40). These VALs may help create holes locally in the PG layers to better expose receptors for irreversible binding and to facilitate the ejection of genetic material into the host's cytoplasm (40).

The whole-genome sequencing revealed the presence of two putative endopeptidase-encoding genes in LC001, but no glycosidase (lysozyme or LT) gene homolog can be identified (Fig. 2; see Table S3 in the supplemental material). Intriguingly, for LC001's host bacterium XH001, spontaneous nonsense mutation or frameshift mutations in *ltg-1*, as well as targeted deletion of *ltg-1*, led to a significantly reduced LC001 binding and LC001 resistance phenotype. *ltg-1* encoded a putative LT enzyme. In bacteria, LTs are regarded as "space-making" autolysins. They catalyze the nonhydrolytic cleavage of the PG structure of the bacterial cell wall and are responsible for creating space within the PG layers for its biosynthesis and recycling, insertion of cell envelope-spanning structures, and cell division. Based on sequence similarity and identified consensus motif, LTs can be classified into four distinct families (32). Bacteria often encode multiple LTs of various families with their substrate preference but also display a certain level of functional redundancy (28). Similarly, at least two more putative LT-encoding genes, *APY09_05140* and *APY09_08845*, were identified, which could explain why *ltg-1* gene mutants exhibited no significant growth defect in the host (Fig. S3). This suggests that compared to other XH001-encoded LTs, Ltg-1 may be more effective in exposing the LC001 receptor as a result of its substrate preference.

The predicted arrangement of the DUF348, G5, and transglycosylase catalytic domains in Ltg-1 (Fig. 3) is highly similar to that in RpfB (30), which is a mycobacterium-encoded lytic transglycosylase, also referred to as resuscitation-promoting factor, that enhances cell growth when added to dormant cultures (31). The bioinformatics analysis also indicated that *ltg-1* encodes a putative membrane-bound family 3 LT enzyme and could be involved in PG recycling and remodeling by catalyzing nonhydrolytic cleavage of the PG structures of the bacterial cell wall (32). Since LC001 itself seemingly lacks LT function, the dynamic remodeling of the PG layer via a bacterial host-encoded LT function could temporarily open the PG layers, expose the receptor(s), and allow the phage to achieve irreversible binding, thus facilitating injection of its genetic material.

In a previous study, a phage T7 *gp16*-encoded LT was shown to be important for effective phage infection against *E. coli*. The absence of gp16 led to significantly delayed internalization of the phage genome (38). Intriguingly, the overexpression of SltY, an *E. coli*-encoded LT, partially rescued the defect in infection of gp16-defective T7. Furthermore, an *sltY* deletion in *E. coli* significantly increases the latent period of wild-type phage T7 (38). Our data are consistent with this finding, suggesting that phages may exploit host-encoded LT enzymatic function to facilitate their infection.

It is worthwhile to point out that while the majority of LC001-resistant mutants display normal growth and carry a mutation in the XH001 *ltg-1* gene, there were few resistant colonies (2 out of 20) showing growth defects. Whole-genome sequencing of these two mutants failed to locate the gene that could be responsible for the LC001-resistant phenotype, due to the large number of polymorphisms detected in many genes. Thus, it remains to be determined if these mutants may carry mutations in the gene that encodes receptor for LC001 while also serving a critical cell wall function whose mutation will lead to a growth defect.

XH001 grown on an agar surface, which is more analogous to a biofilm, was significantly more susceptible to LC001 binding and infection than XH001 grown on planktonic cells, likely due to differential expression of the phage receptor, whose identity remains to be determined. A recent study by Lourenço et al. showed that within the host-associated microbiome, the regulation of bacterial gene expression, such as the expression of phage receptors, may impact the coexistence of phages and their host bacteria (39). The differential

LC001 susceptibility displayed by XH001 under different growth modes, such as planktonic versus biofilm, may promote the long-term coexistence of the two antagonistic interacting partners within the oral cavity, an intriguing question that warrants further investigation.

Due to their inability to carry out biological processes necessary for reproduction, phages have evolved to hijack host machinery and reconfigure host metabolism to optimize phage propagation once their genetic materials are successfully transferred into the host cell (41). Our study presents data showing that some phages have evolved to exploit host-encoded functions to achieve better binding, a significant step ensuring successful infection.

MATERIALS AND METHODS

Bacterial strains and culture conditions. The bacterial strains and plasmids used in this study and their characteristics are listed in Table S1 in the supplemental material. *Schaalia odontolytica* subsp. *actinosynbacter* strain XH001, which was isolated from the human oral cavity (26), and its derivatives were cultured in brain heart infusion (BHI) broth (BD Bacto, Sparks, MD) or 1.5% agar (Fisher Bioreagents, Pittsburgh, PA) at 37°C under microaerophilic conditions (2% O_2, 5% CO_2, 93% N_2). Kanamycin (Kan) (250 μg/mL; Fisher Bioreagents, Pittsburgh, PA) was added to the growth medium for antibiotic selection when appropriate.

Isolation of lytic phage infecting XH001. Saliva sample collection was performed as previously described (42) under Forsyth Institutional Review Board protocol number 21-02. Each sample was vortexed vigorously for 60 s and centrifuged at 7,800 $\times$ *g* for 10 min. The supernatant was passed through a 0.45-μm-pore-size filter, and 5 μL of each filtrate was spotted onto a BHI agar plate with top-agar overlays containing XH001. Plates were incubated under the microaerophilic condition at 37°C and examined after 24 h for lysis zones. The phage within the lysis zone was purified as previously reported (17) and named LC001.

Purification and concentration of LC001 phage particles. LC001 phage particles were propagated by using the double agar overlay plate method as described previously (17). In brief, phage particles in top agar were eluted in Ringer's solution (0.12 g/L calcium chloride, 0.105 g/L potassium chloride, 0.05 g/L sodium bicarbonate, 2.25 g/L sodium chloride, pH 7.4) overnight at 4°C. Phage lysate was collected and filtered through a 0.22-μm-pore-size filter. Phage suspension was treated with chloroform (final concentration, 20%), and then the upper phage-containing suspension was carefully collected after centrifugation at 6,000 $\times$ *g* at 4°C for 10 min. Then, phage particles were treated with polyethylene glycol 8000 (final concentration, 20%) and NaCl (final concentration, 0.5 M) prior to incubation on ice for 30 min. Phage particles were then precipitated by ultracentrifugation at 120,000 $\times$ *g* in a Beckman Coulter type 45 Ti rotor at 4°C for 1 h, and the pellet was resuspended in Ringer's solution. The titer of LC001 was determined using the standard double agar overlay method (43). Briefly, XH001 was used as the host strain to measure the titer of LC001. The supernatant containing LC001 was diluted in 10-fold increments to 10^{-8}. Then, 0.1-mL aliquots of each diluted LC001 supernatant were mixed with 0.1 mL XH001. Each resultant mixture was added to 5 mL of 0.75% BHI soft agar and plated on 1.5% BHI agar plates. The number of PFU was calculated after 24 h of incubation at 37°C under microaerophilic conditions. The phage lysate was stored at 4°C until further use.

Extraction and sequencing of phage DNA. LC001 genomic DNA was extracted from concentrated phage particles by using the phenol and chloroform method (43) and cleaned up with the Wizard DNA clean-up system (Promega, Madison, WI). The DNA pellet was dissolved in TE buffer (10 mM Tris-HCl, 1 mM disodium EDTA, pH 8.0) and stored at −20°C until further use. The DNA was sequenced using the MiSeq Illumina platform (44), and sequences were further annotated by Prokka (45). DNA and protein sequences were scanned for homologs by BLAST.

Host range of LC001. The host range of LC001 was examined by the spot-test lysis method as described previously (17) for its ability to lyse a panel of phylogenetically closely related *Actinomyces* spp., including *Actinomyces meyeri* W712, *Actinomyces graevenitzii* F0530, *Actinomyces georgiae* F0490, *Actinomyces massiliensis* F0489, and *Actinomyces naeslundii*, and two additional *Schaalia odontolytica* strains, ATCC 17982 and F0309 (27). All the tested strains were cultured in BHI medium.

Adsorption assay. To perform the phage adsorption assay, bacterial cells growing in liquid or on an agar plate surface were harvested and resuspended in BHI broth. The optical density at 600 nm (OD_{600}) of the host suspension was adjusted to 1, and 1 mL of host cell suspension was mixed with 100 μL of LC001 phage (approximately 10^4 phage particles), followed by incubation at 37°C for 10 min under shaking. The mixture was then filtered through a 0.22-μm filter, and the number of phages in the filtrate was determined by the plaque assay. The adsorption rate of the phage was calculated by the equation [(titer of added phages − residual titer in filtrate)/(titer of added phages)] $\times$ 100%.

Cryo-ET. (i) Preparation of cryo-ET samples. Agar surface-grown XH001 cells were collected and resuspended in phosphate-buffered saline (PBS) ($\sim 10^9$ cells/mL). One hundred microliters of XH001 cell suspension was mixed with an equal volume of LC001 solution with a titer of 10^{12} PFU/mL, mixed well, and used for subsequent cryo-electron tomography (cryo-ET) sample preparation.

Cryo-ET samples were prepared using copper grids with holey carbon support film (200 mesh, R2/1; Quantifoil). The grids were glow discharged for ~30 s before 5 μL of cell solution was deposited onto them. Then, the grids were blotted with Whatman filter paper from the back side for about 8 s and rapidly plunge-frozen in liquid ethane cooled with liquid nitrogen by using a homemade gravity-driven plunger apparatus (46, 47).

(ii) Cryo-FIB milling. The cryo-focused ion beam (cryo-FIB) milling was performed as previously described (48). Briefly, the plunge-frozen grids were clipped into cryo-FIB autogrids and mounted into the specimen shuttle under liquid nitrogen. Samples were milled to thin lamellae using an Aquilos cryo-FIB system (Thermo Fisher Scientific, Waltham, MA). Samples were sputter coated with platinum to improve the overall sample conductivity, deposited with an organometallic platinum layer (4- to 5-μm thick) using a gas injection system for sample protection, and milled using the gallium ion beam at 30 kV with a stage tilt angle of around 17°. The ion beam current was reduced according to the lamella thickness during the milling process to prevent beam damage and finally polished with a 30-pA ion beam current until a thickness of ~200 nm was reached. Afterward, a thin platinum layer was sputter coated on the lamella to prevent possible charging issues during the cryo-ET imaging. Then, the grids were saved in liquid nitrogen until used for cryo-ET data collection.

(iii) Cryo-ET data acquisition and tomogram reconstruction. The cryo-FIB lamellae were transferred to a 300-kV Titan Krios electron microscope (Thermo Fisher Scientific, Waltham, MA) equipped with a direct electron detector, Volta phase plate (VPP), and energy filter (Gatan). SerialEM (49) was used to collect single-axis tilt series around 0-μm defocus with VPP, with a cumulative dose of ~90 e^-/Å covering tilt angles from −51° to 51° (3° tilt step). Images were acquired with an effective pixel size of 3.384 Å at the specimen level. All recorded images were first drift corrected by the software MotionCor2 (50) and then stacked by the software package IMOD (51). The tilt series was aligned by IMOD with the patching tracking method, followed by reconstruction of the tomograms in IMOD using the aligned stacks.

(iv) Subtomogram averaging and three-dimensional visualization of LC001. Four tomograms were collected from pure LC001 samples. LC001 particles were manually picked from the 6× binned tomograms (as described in reference 52). The subtomograms of LC001 were first extracted from the bin6 tomograms, and then the i3 software package (53, 54) was used for three-dimensional (3D) alignment and classification to get refined particle positions and to remove junk particles. Afterward, the subtomograms were extracted from unbinned tomograms with the refined positions and further binned by 2 or 4 based on the requirement for alignment and classification. In total, 436 subtomograms of LC001 were selected from the tomographic reconstructions and used for subtomogram analysis. UCSF ChimeraX (55) was used for surface rendering of LC001 subtomogram average structure.

Isolation and whole-genome sequencing of spontaneous LC001-resistant XH001 mutants. Wild-type XH001 cells were harvested at the exponential growth phase and resuspended in PBS to a final concentration of 10^9 cells/mL. The XH001 suspension was mixed with LC001 at an MOI of approximately 1:100. The mixture was plated on BHI agar plates and incubated at 37°C for 7 days under microaerobic conditions. Putative LC001-resistant mutants grown as colonies on the plates were picked and streak purified. Their LC001-resistant phenotype was confirmed by the spot-test lysis method (17). Once confirmed, stocks of the mutants were prepared and stored at −80°C in 20% glycerol for later use.

Genomic DNA of the spontaneous LC001-resistant mutants was isolated and subjected to full genome sequencing. A genomic comparative analysis of XH001 and its phage-resistant mutants was performed by Breseq (56). The *Schaalia odontolytica* strain XH001 genome (GenBank accession no. LLVT00000000.1; BioProject accession no. PRJNA298751) was used as a reference.

Generation of an *ltg-1* deletion mutant in XH001 via allelic replacement. The chromosomal gene deletion mutant of *ltg-1* was generated by following previously described protocols (25, 57) via fusion PCR (58). The respective 1-kb up/downstream homology gene fragments of the *ltg-1* gene (primers 1/2 and 5/6), as well as the kanamycin gene resistance cassette (primers 3/4) from pJDR215 (59) were PCR amplified and fused using the corresponding primers listed in Table S2. The resulting linear fragment generated was purified and concentrated via gel extraction with the QIAquick gel extraction kit (Qiagen, Hilden Germany), followed by the DNA Clean & Concentrator kit (Zymo Research DNA Clean & Concentrator catalog no. D4013), in accordance with the manufacturers' instructions. The Phusion hi-fidelity PCR master mix with GC buffer was used for PCR amplification of the resulting *ltg-1* gene deletion construct (primers 1/6), in accordance with the manufacturer's protocol, to generate sufficient product prior to transformation (25) and allelic replacement of *ltg-1* in XH001. Putative XH001ΔLT mutants were evaluated for allelic replacement of the *ltg-1* gene with the kanamycin cassette (primers 7/8) in comparison to the WT (primers 9/10) sequence via DNA sequencing. The sequence-confirmed mutants were further screened for ablation of mRNA expression in the XH001 Δ*ltg-1* background as previously described (57).

Visualization and quantification of attachment of LC001 to XH001. Differences in phage adsorption to XH001 wild type and its mutant derivatives were visualized using previously described SYBR green labeling with minor modification (60). Briefly, isolated LC001 phage particles (phage titer, 10^{11} PFU/mL) were mixed 1,000:1 (vol/vol) with a 10-fold-diluted SYBR gold stock solution ((Invitrogen, Waltham, MA) and incubated overnight in the dark at 4°C). XH001 and its derivatives were grown overnight on BHI agar plates, scraped off, adjusted to an OD_{600} of 0.5 (10^8 cells/mL) in Ringer solution, stained with 4 μM Laurdan (Invitrogen, Waltham, MA) for 30 min, and washed again twice with Ringer solution. Laurdan-stained bacterial cells were then mixed with SYBR gold-stained LC001 at MOIs of approximately 1:100. The mixtures were incubated at room temperature for 10 min and visualized with a confocal microscope (LSM880; Zeiss, Germany) through a 63×, 1.4-numerical-aperture Plan-Apochromat objective. Five representative images were acquired for each group and processed with Fiji 2.1.0 (61).

Phage binding patterns were analyzed and quantified via Fiji particle analysis. Fluorescence signals from Laurdan-stained bacterial cells (488-nm excitation, emission collected with a bandpass filter from 500 to 550 nm) were converted into binary format and segmented with the same threshold for all images. Fluorescence signals from SYBR green-stained LC001 (405-nm excitation, emission collected with a bandpass filter from 420 to 470 nm) were then redirected to the segmented Laurdan (bacterial) channel. The particle area value (referred to as the absolute phage particle intensity) within the

segmented host area, as well as the particle area fraction [referred to as the (phage area/segmented host area) × 100%], was calculated and plotted as a histogram in GraphPad Prism 8.0. Six views from biological duplicate experiments were analyzed for each group. The unpaired *t* test was performed to compare the binding between LC001 and different XH001 wild-type and mutant strains.

Complementation of *ltg-1* mutant strain. A sequence including *ltg-1* and 100 bp upstream of its predicted start codon (containing the ribosomal binding site) was amplified from XH001 with *Taq* DNA polymerase using forward (LTC-F1, 5′-GACTCTGGGGTTCGCCTCGATCTGACGTGACATTGCACGCG-3′) and reverse (LTC-R1, 5′-GCTTGGTCGGTCATTTCGCCTTAGTACCAGCCCACGGCATT-3′) primers and subcloned into XhoI-digested pJRD215 using the GeneArt seamless cloning and assembly kit (Thermo Fisher Scientific, Waltham, WA). The pJRD215 derivative carrying *ltg-1*, named pCLJ100, was transformed into XH001 LR-01 (a spontaneous LC001 resistance mutant with a nonsense mutation in *ltg-1*). Transformants were selected on Kan-containing agar plates and confirmed by diagnostic PCR using the primer set Diag-1F (ATGGATTGCACGCAGGTTC) and Diag-1R (TTAGTACCAGCCCACGGCATT) with a predicted size of 2,300 bp. The new derivative strain, XH001 LR-01(pCLJ100), was subjected to testing of its phage LC001 sensitivity.

qRT-PCR. Bacteria were cultured in BHI liquid or on agar plates at 37°C. The bacteria cultured in liquid were collected by centrifugation and resuspended in BHI at an OD_{600} of 0.5, while the surface-grown bacteria were scraped from the plate, resuspended in BHI, and adjusted to an OD_{600} of 0.5. The same volumes of resuspended planktonic and surface-grown cells were subjected to centrifugation to collect bacterial cells. Quantitative real-time reverse transcription PCR (qRT-PCR) was performed as previously described (62). Briefly, the total RNA was extracted using TRIzol (Thermo Fisher Scientific, USA) according to the manufacturer's instructions. RNA was reverse transcribed, and qRT-PCR was performed using SYBR Premix Ex Taq II (TaKaRa Bio, China) with primers ltg-1F (ATGAACACGAGCATGATC) and ltg-1R (CTATTCGGCGTACTTCCT). The level of 16S rRNA transcript was determined using primers XH-F5 (GCGGAGCATGCGGATTA) and XH-R3 (AACGTGCTGGCAACATAGGG) and used to normalize the gene expression data.

Statistical analyses. Student's *t* test was used to compare two-group data. A *P* value of <0.05 was considered statistically significant.

Data availability. The genome sequence of the *Schaalia odontolytica* phage LC001 is available in GenBank under accession number ON920540.1.

SUPPLEMENTAL MATERIAL

Supplemental material is available online only.

SUPPLEMENTAL FILE 1, PDF file, 6.1 MB.

SUPPLEMENTAL FILE 2, XLS file, 0.1 MB.

ACKNOWLEDGMENTS

The study was in part supported by NIH/NIDCR grant no. R01DE023810 (X.H., J.S.M.), R01DE030943 (X.H.), 3R01DE023810-07S1 (X.H., J.L.) and F31DE026057 (J.B.) and the National Natural Science Foundation of China (NSFC grant no. 31870167 to S.L.). We thank Meng Shao for preparing cryo-ET samples with cryo-FIB/SEM at the Liu laboratory at Yale; Y.C. and J.L. were supported by grants R01AI087946 and R01AI132818 from the National Institute of Allergy and Infectious Diseases (NIAID); Cryo-ET data were collected at the Yale Cryo-EM resources and funded in part by the NIH grant 1S10OD023603-01A1.

We declare that there are no competing financial interests in relation to the work described.

REFERENCES

1. Fernandez L, Rodriguez A, Garcia P. 2018. Phage or foe: an insight into the impact of viral predation on microbial communities. ISME J 12:1171–1179. https://doi.org/10.1038/s41396-018-0049-5.
2. Koskella B, Brockhurst MA. 2014. Bacteria-phage coevolution as a driver of ecological and evolutionary processes in microbial communities. FEMS Microbiol Rev 38:916–931. https://doi.org/10.1111/1574-6976.12072.
3. Suttle CA. 2007. Marine viruses—major players in the global ecosystem. Nat Rev Microbiol 5:801–812. https://doi.org/10.1038/nrmicro1750.
4. Shkoporov AN, Clooney AG, Sutton TDS, Ryan FJ, Daly KM, Nolan JA, McDonnell SA, Khokhlova EV, Draper LA, Forde A, Guerin E, Velayudhan V, Ross RP, Hill C. 2019. The human gut virome is highly diverse, stable, and individual specific. Cell Host Microbe 26:527–541.e5. https://doi.org/10.1016/j.chom.2019.09.009.
5. Camarillo-Guerrero LF, Almeida A, Rangel-Pineros G, Finn RD, Lawley TD. 2021. Massive expansion of human gut bacteriophage diversity. Cell 184:1098–1109.e9. https://doi.org/10.1016/j.cell.2021.01.029.
6. Szafrański SP, Slots J, Stiesch M. 2021. The human oral phageome. Periodontol 2000 86:79–96. https://doi.org/10.1111/prd.12363.
7. Kuramitsu HK, He X, Lux R, Anderson MH, Shi W. 2007. Interspecies interactions within oral microbial communities. Microbiol Mol Biol Rev 71:653–670. https://doi.org/10.1128/MMBR.00024-07.
8. Chen T, Yu W-H, Izard J, Baranova OV, Lakshmanan A, Dewhirst FE. 2010. The Human Oral Microbiome Database: a web accessible resource for investigating oral microbe taxonomic and genomic information. Database (Oxford) 2010:baq013. https://doi.org/10.1093/database/baq013.
9. Baker JL, Bor B, Agnello M, Shi W, He X. 2017. Ecology of the oral microbiome: beyond bacteria. Trends Microbiol 25:362–374. https://doi.org/10.1016/j.tim.2016.12.012.
10. Meyers CE, Walter EL, Green LB. 1958. Isolation of a bacteriophage specific for a Lactobacillus casei from human oral material. J Dent Res 37:175–178. https://doi.org/10.1177/00220345580370011201.
11. Olsen I, Namork E, Myhrvold V. 1993. Electron microscopy of phages in serotypes of Actinobacillus actinomycetemcomitans. Oral Microbiol Immunol 8:383–385. https://doi.org/10.1111/j.1399-302x.1993.tb00615.x.
12. Khalifa L, Brosh Y, Gelman D, Coppenhagen-Glazer S, Beyth S, Poradosu-Cohen R, Que Y-A, Beyth N, Hazan R. 2015. Targeting Enterococcus

faecalis biofilms with phage therapy. Appl Environ Microbiol 81:2696–2705. https://doi.org/10.1128/AEM.00096-15.
13. Hiroki H, Shiiki J, Handa A, Totsuka M, Nakamura O. 1976. Isolation of bacteriophages specific for the genus Veillonella. Arch Oral Biol 21:215–217. https://doi.org/10.1016/0003-9969(76)90132-1.
14. Dalmasso M, de Haas E, Neve H, Strain R, Cousin FJ, Stockdale SR, Ross RP, Hill C. 2015. Isolation of a novel phage with activity against Streptococcus mutans biofilms. PLoS One 10:e0138651. https://doi.org/10.1371/journal.pone.0138651.
15. Machuca P, Daille L, Vinés E, Berrocal L, Bittner M. 2010. Isolation of a novel bacteriophage specific for the periodontal pathogen Fusobacterium nucleatum. Appl Environ Microbiol 76:7243–7250. https://doi.org/10.1128/AEM.01135-10.
16. Mitchell HL, Dashper SG, Catmull DV, Paolini RA, Cleal SM, Slakeski N, Tan KH, Reynolds EC. 2010. Treponema denticola biofilm-induced expression of a bacteriophage, toxin-antitoxin systems and transposases. Microbiology (Reading) 156:774–788. https://doi.org/10.1099/mic.0.033654-0.
17. Tylenda CA, Calvert C, Kolenbrander PE, Tylenda A. 1985. Isolation of Actinomyces bacteriophage from human dental plaque. Infect Immun 49:1–6. https://doi.org/10.1128/iai.49.1.1-6.1985.
18. Szafrański SP, Winkel A, Stiesch M. 2017. The use of bacteriophages to biocontrol oral biofilms. J Biotechnol 250:29–44. https://doi.org/10.1016/j.jbiotec.2017.01.002.
19. Abeles SR, Robles-Sikisaka R, Ly M, Lum AG, Salzman J, Boehm TK, Pride DT. 2014. Human oral viruses are personal, persistent and gender-consistent. ISME J 8:1753–1767. https://doi.org/10.1038/ismej.2014.31.
20. Ly M, Abeles SR, Boehm TK, Robles-Sikisaka R, Naidu M, Santiago-Rodriguez T, Pride DT. 2014. Altered oral viral ecology in association with periodontal disease. mBio 5:e01133-14. https://doi.org/10.1128/mBio.01133-14.
21. Naidu M, Robles-Sikisaka R, Abeles SR, Boehm TK, Pride DT. 2014. Characterization of bacteriophage communities and CRISPR profiles from dental plaque. BMC Microbiol 14:175. https://doi.org/10.1186/1471-2180-14-175.
22. Pride DT, Salzman J, Haynes M, Rohwer F, Davis-Long C, White RA, Loomer P, Armitage GC, Relman DA. 2012. Evidence of a robust resident bacteriophage population revealed through analysis of the human salivary virome. ISME J 6:915–926. https://doi.org/10.1038/ismej.2011.169.
23. Edlund A, Santiago-Rodriguez TM, Boehm TK, Pride DT. 2015. *Bacteriophage and their potential roles in the human oral cavity*. J Oral Microbiol 7:27423. https://doi.org/10.3402/jom.v7.27423.
24. McLean JS, Liu Q, Bor B, Bedree JK, Cen L, Watling M, To TT, Bumgarner RE, He X, Shi W. 2016. Draft genome sequence of Actinomyces odontolyticus subsp. actinosynbacter strain XH001, the basibiont of an oral TM7 epibiont. Genome Announc 4:e01685-15. https://doi.org/10.1128/genomeA.01685-15.
25. Bedree JK, Bor B, Cen L, Edlund A, Lux R, McLean JS, Shi W, He X. 2018. Quorum sensing modulates the epibiotic-parasitic relationship between Actinomyces odontolyticus and its Saccharibacteria epibiont, a Nanosynbacter lyticus strain, TM7x. Front Microbiol 9:2049. https://doi.org/10.3389/fmicb.2018.02049.
26. He X, McLean JS, Edlund A, Yooseph S, Hall AP, Liu S-Y, Dorrestein PC, Esquenazi E, Hunter RC, Cheng G, Nelson KE, Lux R, Shi W. 2015. Cultivation of a human-associated TM7 phylotype reveals a reduced genome and epibiotic parasitic lifestyle. Proc Natl Acad Sci U S A 112:244–249. https://doi.org/10.1073/pnas.1419038112.
27. Tian J. 2022. Acquisition of the arginine deiminase system benefits epiparasitic Saccharibacteria and their host bacteria in a mammalian niche environment. Proc Natl Acad Sci U S A 119:e2114909119. https://doi.org/10.1073/pnas.2114909119.
28. Dik DA, Marous DR, Fisher JF, Mobashery S. 2017. Lytic transglycosylases: concinnity in concision of the bacterial cell wall. Crit Rev Biochem Mol Biol 52:503–542. https://doi.org/10.1080/10409238.2017.1337705.
29. Mulder N, Apweiler R. 2007. InterPro and InterProScan: tools for protein sequence classification and comparison. Methods Mol Biol 396:59–70. https://doi.org/10.1007/978-1-59745-515-2_5.
30. Ruggiero A, Squeglia F, Romano M, Vitagliano L, De Simone A, Berisio R. 2016. The structure of Resuscitation promoting factor B from M. tuberculosis reveals unexpected ubiquitin-like domains. Biochim Biophys Acta 1860:445–451. https://doi.org/10.1016/j.bbagen.2015.11.001.
31. Hett EC, Chao MC, Deng LL, Rubin EJ. 2008. A mycobacterial enzyme essential for cell division synergizes with resuscitation-promoting factor. PLoS Pathog 4:e1000001. https://doi.org/10.1371/journal.ppat.1000001.
32. Scheurwater E, Reid CW, Clarke AJ. 2008. Lytic transglycosylases: bacterial space-making autolysins. Int J Biochem Cell Biol 40:586–591. https://doi.org/10.1016/j.biocel.2007.03.018.
33. Thunnissen AM, Dijkstra AJ, Kalk KH, Rozeboom HJ, Engel H, Keck W, Dijkstra BW. 1994. Doughnut-shaped structure of a bacterial muramidase revealed by X-ray crystallography. Nature 367:750–753. https://doi.org/10.1038/367750a0.
34. Thunnissen AM, Rozeboom HJ, Kalk KH, Dijkstra BW. 1995. Structure of the 70-kDa soluble lytic transglycosylase complexed with bulgecin A. Implications for the enzymatic mechanism. Biochemistry 34:12729–12737. https://doi.org/10.1021/bi00039a032.
35. van Asselt EJ, Thunnissen AM, Dijkstra BW. 1999. High resolution crystal structures of the Escherichia coli lytic transglycosylase Slt70 and its complex with a peptidoglycan fragment. J Mol Biol 291:877–898. https://doi.org/10.1006/jmbi.1999.3013.
36. Dijkstra AJ, Keck W. 1996. Peptidoglycan as a barrier to transenvelope transport. J Bacteriol 178:5555–5562. https://doi.org/10.1128/jb.178.19.5555-5562.1996.
37. Bertozzi Silva J, Storms Z, Sauvageau D. 2016. Host receptors for bacteriophage adsorption. FEMS Microbiol Lett 363:fnw002. https://doi.org/10.1093/femsle/fnw002.
38. Moak M, Molineux IJ. 2000. Role of the Gp16 lytic transglycosylase motif in bacteriophage T7 virions at the initiation of infection. Mol Microbiol 37:345–355. https://doi.org/10.1046/j.1365-2958.2000.01995.x.
39. Lourenço M, Chaffringeon L, Lamy-Besnier Q, Titécat M, Pédron T, Sismeiro O, Legendre R, Varet H, Coppée JY, Bérard M, De Sordi L, Debarbieux L. 2022. The gut environment regulates bacterial gene expression which modulates susceptibility to bacteriophage infection. Cell Host Microbe 30:556–569.e5. https://doi.org/10.1016/j.chom.2022.03.014.
40. Latka A, Maciejewska B, Majkowska-Skrobek G, Briers Y, Drulis-Kawa Z. 2017. Bacteriophage-encoded virion-associated enzymes to overcome the carbohydrate barriers during the infection process. Appl Microbiol Biotechnol 101:3103–3119. https://doi.org/10.1007/s00253-017-8224-6.
41. Warwick-Dugdale J, Buchholz HH, Allen MJ, Temperton B. 2019. Host-hijacking and planktonic piracy: how phages command the microbial high seas. Virol J 16:15. https://doi.org/10.1186/s12985-019-1120-1.
42. Tian Y, He X, Torralba M, Yooseph S, Nelson KE, Lux R, McLean JS, Yu G, Shi W. 2010. Using DGGE profiling to develop a novel culture medium suitable for oral microbial communities. Mol Oral Microbiol 25:357–367. https://doi.org/10.1111/j.2041-1014.2010.00585.x.
43. Shen M, Yang Y, Shen W, Cen L, McLean JS, Shi W, Le S, He X. 2018. A linear plasmid-like prophage of Actinomyces odontolyticus promotes biofilm assembly. Appl Environ Microbiol 84:e01263-18. https://doi.org/10.1128/AEM.01263-18.
44. Bor B, McLean JS, Foster KR, Cen L, To TT, Serrato-Guillen A, Dewhirst FE, Shi W, He X. 2018. Rapid evolution of decreased host susceptibility drives a stable relationship between ultrasmall parasite TM7x and its bacterial host. Proc Natl Acad Sci U S A 115:12277–12282. https://doi.org/10.1073/pnas.1810625115.
45. Seemann T. 2014. Prokka: rapid prokaryotic genome annotation. Bioinformatics 30:2068–2069. https://doi.org/10.1093/bioinformatics/btu153.
46. Liu J, Lin T, Botkin DJ, McCrum E, Winkler H, Norris SJ. 2009. Intact flagellar motor of Borrelia burgdorferi revealed by cryo-electron tomography: evidence for stator ring curvature and rotor/C-ring assembly flexion. J Bacteriol 191:5026–5036. https://doi.org/10.1128/JB.00340-09.
47. Zhao X, Zhang K, Boquoi T, Hu B, Motaleb MA, Miller KA, James ME, Charon NW, Manson MD, Norris SJ, Li C, Liu J. 2013. Cryoelectron tomography reveals the sequential assembly of bacterial flagella in Borrelia burgdorferi. Proc Natl Acad Sci U S A 110:14390–14395. https://doi.org/10.1073/pnas.1308306110.
48. Xiang Y, Surovtsev IV, Chang Y, Govers SK, Parry BR, Liu J, Jacobs-Wagner C. 2021. Interconnecting solvent quality, transcription, and chromosome folding in Escherichia coli. Cell 184:3626–3642.e14. https://doi.org/10.1016/j.cell.2021.05.037.
49. Mastronarde DN. 2005. Automated electron microscope tomography using robust prediction of specimen movements. J Struct Biol 152:36–51. https://doi.org/10.1016/j.jsb.2005.07.007.
50. Zheng SQ, Palovcak E, Armache J-P, Verba KA, Cheng Y, Agard DA. 2017. MotionCor2: anisotropic correction of beam-induced motion for improved cryo-electron microscopy. Nat Methods 14:331–332. https://doi.org/10.1038/nmeth.4193.
51. Kremer JR, Mastronarde DN, McIntosh JR. 1996. Computer visualization of three-dimensional image data using IMOD. J Struct Biol 116:71–76. https://doi.org/10.1006/jsbi.1996.0013.
52. Zhu S, Qin Z, Wang J, Morado DR, Liu J. 2017. In situ structural analysis of the spirochetal flagellar motor by cryo-electron tomography. Methods Mol Biol 1593:229–242. https://doi.org/10.1007/978-1-4939-6927-2_18.
53. Winkler H. 2007. 3D reconstruction and processing of volumetric data in cryo-electron tomography. J Struct Biol 157:126–137. https://doi.org/10.1016/j.jsb.2006.07.014.

54. Winkler H, Zhu P, Liu J, Ye F, Roux KH, Taylor KA. 2009. Tomographic subvolume alignment and subvolume classification applied to myosin V and SIV envelope spikes. J Struct Biol 165:64–77. https://doi.org/10.1016/j.jsb.2008.10.004.
55. Goddard TD, Huang CC, Meng EC, Pettersen EF, Couch GS, Morris JH, Ferrin TE. 2018. UCSF ChimeraX: meeting modern challenges in visualization and analysis. Protein Sci 27:14–25. https://doi.org/10.1002/pro.3235.
56. Barrick JE, Colburn G, Deatherage DE, Traverse CC, Strand MD, Borges JJ, Knoester DB, Reba A, Meyer AG. 2014. Identifying structural variation in haploid microbial genomes from short-read resequencing data using breseq. BMC Genomics 15:1039. https://doi.org/10.1186/1471-2164-15-1039.
57. Chipashvili O, Utter DR, Bedree JK, Ma Y, Schulte F, Mascarin G, Alayyoubi Y, Chouhan D, Hardt M, Bidlack F, Hasturk H, He X, McLean JS, Bor B. 2021. Episymbiotic Saccharibacteria suppresses gingival inflammation and bone loss in mice through host bacterial modulation. Cell Host Microbe 29:1649–1662.e7. https://doi.org/10.1016/j.chom.2021.09.009.
58. Shevchuk NA, Bryksin AV, Nusinovich YA, Cabello FC, Sutherland M, Ladisch S. 2004. Construction of long DNA molecules using long PCR-based fusion of several fragments simultaneously. Nucleic Acids Res 32:e19. https://doi.org/10.1093/nar/gnh014.
59. Yeung MK, Kozelsky CS. 1994. Transformation of Actinomyces spp. by a gram-negative broad-host-range plasmid. J Bacteriol 176:4173–4176. https://doi.org/10.1128/jb.176.13.4173-4176.1994.
60. Szymczak P, Filipe SR, Covas G, Vogensen FK, Neves AR, Janzen T. 2018. Cell wall glycans mediate recognition of the dairy bacterium Streptococcus thermophilus by bacteriophages. Appl Environ Microbiol 84:e01847-18. https://doi.org/10.1128/AEM.01847-18.
61. Schindelin J, Arganda-Carreras I, Frise E, Kaynig V, Longair M, Pietzsch T, Preibisch S, Rueden C, Saalfeld S, Schmid B, Tinevez J-Y, White DJ, Hartenstein V, Eliceiri K, Tomancak P, Cardona A. 2012. Fiji: an open-source platform for biological-image analysis. Nat Methods 9:676–682. https://doi.org/10.1038/nmeth.2019.
62. Zhong Q, Yang L, Li L, Shen W, Li Y, Xu H, Zhong Z, Chen M, Le S. 2020. Transcriptomic analysis reveals the dependency of Pseudomonas aeruginosa genes for double-stranded RNA bacteriophage phiYY infection cycle. iScience 23:101437. https://doi.org/10.1016/j.isci.2020.101437.